Science Bulletin xxx (xxxx) xxx

Contents lists available at ScienceDirect

Science Bulletin

journal homepage: www.elsevier.com/locate/scib

Article

Decadal climate control of circulation regime transitions in a large marginal sea

Lixia Zheng [a,b,c], Zhongya Cai [a,b,*], Jianping Gan [b,d,e,*], Chiwing Hui [b,d], Linlin Liang [b,e], Hiusuet Kung [b,d], Zhiqiang Liu [f]

[a] State Key Laboratory of Internet of Things for Smart City and Department of Ocean Science and Engineering, University of Macau, Macau 999078, China
[b] Center for Ocean Research in Hong Kong and Macau, Hong Kong University of Science and Technology, Hong Kong 999077, China
[c] Southern Marine Science and Engineering Guandong Laboratory (Zhuhai), Zhuhai 519000, China
[d] Department of Ocean Science and Department of Mathematics, Hong Kong University of Science and Technology, Hong Kong 999077, China
[e] Earth, Ocean and Atmospheric Sciences Thrust, The Hong Kong University of Science and Technology (Guangzhou), Guangzhou 510000, China
[f] Department of Ocean Science and Engineering, Southern University of Science and Technology, Shenzhen 511464, China

ARTICLE INFO

Article history:
Received 7 July 2025
Received in revised form 2 December 2025
Accepted 3 December 2025
Available online xxxx

Keywords:
Marginal sea circulation
Regime transition
Decadal oscillation
Layered circulation

ABSTRACT

Marginal seas, as transitional zones, are closely connected to the open ocean and adjacent coastal systems. Their circulations often exhibit strong oscillatory behavior that shapes heat and salt transport, nutrient cycling, and regional ocean–atmosphere interactions. However, the characteristics and underlying dynamics of these oscillations remain insufficiently understood. Using the unique three-layer alternating circulation in the South China Sea as an example, we show that the system undergoes a pronounced regime transition from 1993–2008 to 2009–2018. This transition is closely linked to the phase change of the Pacific Decadal Oscillation. Specifically, upper-layer cyclonic circulation intensifies during the pre-2009 but weakens during the post-2009 period, while the middle-layer anticyclonic circulation exhibits the opposite pattern. In contrast, the deep-layer circulation strengthens substantially during the post-2009 period. These regime transitions arise from the interplay of surface wind forcing, the external exchanging current with the Pacific, and topographically modulated internal vertical coupling. The decadal trend of the upper-layer circulation is primarily wind-driven. The weakening of middle-layer circulation during pre-2009 is governed by pressure torque influenced by the upper-layer, whereas its post-2009 strengthening is attributed to vortex stretching associated with enhanced deep intrusion from the Pacific and a stronger deep-layer circulation. The findings clarify the oscillatory nature of South China Sea layered circulation under climate variability and highlight its role in regulating regional mass transport and ocean–atmosphere interaction.

1. Introduction

Global marginal seas are separated from major ocean basins by topographic features and are closely connected to the open ocean and adjacent coastal systems. The circulations in marginal seas play a critical role in regulating both regional and global climates by facilitating the exchanges of heat, salinity, nutrients, and carbon between the marginal seas and the open ocean [1–3]. These processes, in turn, influence the sustainability of the environment and socioeconomic activities in neighboring coastal regions.

The South China Sea (SCS), situated within the Indo-Pacific warm pool (Fig. 1a), is bordered by the most densely populated regions and serves as a key pathway for water exchange between the Pacific and Indian Oceans [4–6]. Forced by the Asian monsoon and exchanging current through the surrounding straits, the SCS features a unique layered circulation over its meandering bottom slope. This circulation is characterized by cyclonic-anticyclonic-cyclonic (CAC) circulations in the upper (< 750 m), middle (750–1500 m), and deep layers (> 1500 m), respectively (Fig. 1b–d) [7–15]. The upper-layer circulation is primarily controlled by the local wind forcing and the Kuroshio Current (KC) intrusion from the Western Pacific Ocean (WPO) through the Luzon Strait (Fig. 1a) [2]. The KC originates from the bifurcation of westward-flowing North Equatorial Current upon reaching the Philippine

* Corresponding authors.
E-mail addresses: zycai@um.edu.mo (Z. Cai), magan@ust.hk (J. Gan).

https://doi.org/10.1016/j.scib.2025.12.033
2095-9273/

Please cite this article as: L. Zheng, Z. Cai, J. Gan et al., Decadal climate control of circulation regime transitions in a large marginal sea, Science Bulletin, https://doi.org/10.1016/j.scib.2025.12.033

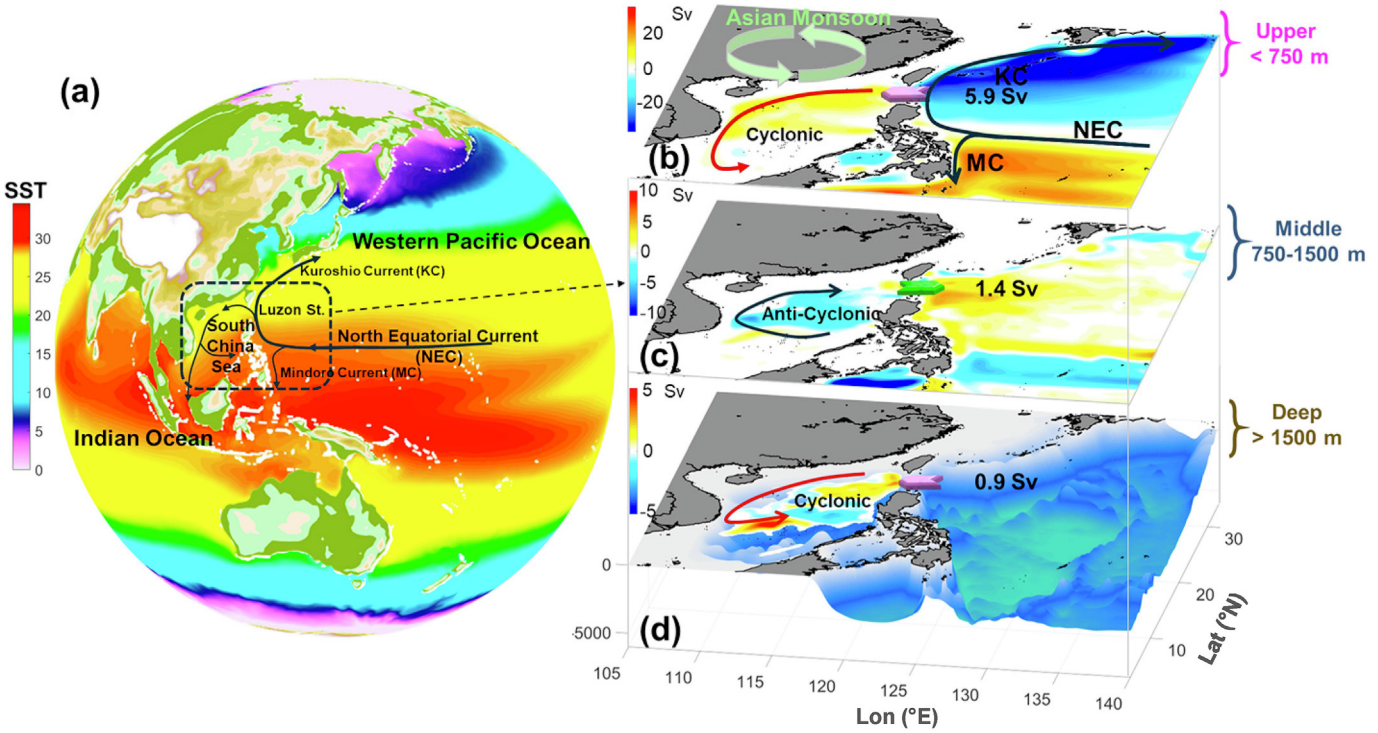

Fig. 1. Characteristics of the layered circulation in the SCS. (a) Schematic representation of the surface circulation (black arrows) and sea surface temperature (SST, °C, color shading) over the SCS and WPO. (b–d) Characteristics of the layered circulation in the SCS and the layered exchanging current in the Luzon Strait (purple and green arrows). The color represents the transport streamfunction for the upper (0–750 m), middle (750–1500 m), and deep (1500 m to bottom) layers, based on CMOMS results. The positive/negative values denote circulation in cyclonic/anticyclonic direction, respectively. The solid arrows show the direction of the mean circulation in SCS and WPO. The volume transport through the Luzon Strait is 5.9 Sv (10^6 m^3 s^{-1}) (influx) in the upper layer, −1.4 Sv (outflux) in the middle layer, and 0.9 Sv (influx) in the deep layer [8].

coast (Fig. 1a). The middle and deep circulations within the semi-enclosed SCS basin are maintained by the outflow and deep intrusion through the Luzon Strait [3,10,13,16,17]. The interactions among currents across these layers, particularly over slope topography, further modulate the structure and intensity of the overall circulation within the SCS [9–11,18].

Located within the Indo-Pacific region, the SCS is exposed to a wide range of climatic variability across multiple spatiotemporal scales through both the atmospheric and oceanic pathways [2,19–22]. Influences from these interactions have led to significant decadal variability in forcing factors [23–26]. Meanwhile, internal dynamics regulated by local topography and thermohaline structure [7,27–29] further shape how the basin circulation responds to external climate signals. The interplay among these factors leads to significant oscillations, often exhibiting stronger signals compared to the global mean [30,31], and even causing trend reversals in regional circulation systems [24,32,33]. For instance, sea levels in the SCS and WPO have oscillated between falling and rising on a decadal scale [24], and surface western boundary current in SCS has undergone weak–strong–weak phase shifts during winter over the past several decades [34].

Such oscillating behavior of marginal sea circulation significantly influences the regional heat and salt transport, nutrient cycling, and ocean-atmosphere interactions. Similar behavior occurs in other regions as well. In the Subpolar North Atlantic basin, under the local circulation shift, the decade-long cooling trend since 2006 rapidly reversed in 2016 [32]. Similarly, sea temperature in the southwestern Gulf of Mexico exhibits the decadal to multidecadal-scale oscillations between warming and cooling [35]. These reversals are closely linked to significant variations in the physical and biogeochemical properties of the local water masses [36,37]. Understanding these reversible oscillations in marginal seas is therefore essential for characterizing ocean functioning and evolution, and for enhancing the predictability of interior ocean dynamics. Previous investigations have largely focused on long-term net trends in circulation and thermodynamic properties, while paying less attention to the nature and mechanisms of these oscillations. Limitations in observational coverage across space and time also hindered a clear understanding of the three-dimensional oscillatory dynamics of the SCS. In this study, utilizing observations, reanalysis products, and rigorously validated model results, we demonstrate and explain significant regime transitions of the rotating layered circulation of the SCS over the past decades.

2. Materials and methods

2.1. Data

The simulation results from the China Sea Multi-scale Ocean Modeling System (CMOMS) [7,8], developed based on the Regional Ocean Modeling System (ROMS) [38], are used in this study. The CMOMS model domain covers the northwest Pacific Ocean (NPO) and all adjacent South China Sea, extending from 0.95°N, 99°E to 50°N, 145°E. The horizontal grid size of the model decreases gradually from ~10 km in the southern part to ~7 km in the northern part of the domain. Additional details regarding the CMOMS configuration are provided in the Supplementary material. The model has been rigorously validated using the geostrophic currents derived from Generalized Digital Environmental Model [7], satellite altimetry data (Figs. S1–S3 online) and geophysical fluid dynamics [7–9], which establishes the reliability of following investigations. In the following analysis, we use 30 years daily results from 1993 to 2022.

Besides the CMOMS simulation, the daily sea-level anomaly with a 0.125° horizontal resolution during 1993–2022 is obtained from the Copernicus Marine Environment Monitoring Service (CMEMS). These data merge observations from multiple satellite altimetry missions (TOPEX/Poseidon, ERS-1/2, Jason-1, Jason-2, and Envisat). Monthly subsurface temperature and salinity field with a 1° horizontal resolution during 1993–2022 from EN4 are used to calculate the density difference across the Luzon Strait between two regions (118°–121°E, 18°–22°N and 121°–124°E, 18°–22°N). To ensure reliability, only data above 3000 m are used in the calculation. Global monthly wind stress with a 0.25° horizontal resolution is derived from the Ocean Reanalysis System 5 (ORAS5).

2.2. Stokes' Theorem based analyses

Based on Stokes' Circulation Theorem, the domain-integrated vorticity in each layer, reflecting the circulation direction and intensity, is defined as:

$$\mathbf{\Gamma} = \oint \int_{\boldsymbol{Lb}}^{\boldsymbol{Lu}} \vec{\boldsymbol{V}} \mathbf{dzd}\boldsymbol{l} = \oiint \nabla \times \int_{\boldsymbol{Lb}}^{\boldsymbol{Lu}} \vec{\boldsymbol{V}} \mathbf{dzd}\boldsymbol{A}, \tag{1}$$

where $\vec{\boldsymbol{V}}$ is the horizontal velocity field, composed of the zonal velocity u and the meridional velocity v, $\boldsymbol{Lu}$ and $\boldsymbol{Lb}$ are the depths of the top and bottom in each layer. Three layers are separated using 750 and 1500 m, following previous investigations [7,39]. Using output from CMOMS, which follows the Arakawa C-grid structure of ROMS, vorticity is calculated at the ψ-points. Grid points directly adjacent to land are masked out and excluded from the calculation of $\mathbf{\Gamma}$. The obtained $\mathbf{\Gamma}$ represents the basin circulation for each layer integrated along the boundary l of the SCS basin. In the following analysis, the $\mathbf{\Gamma}$ is used as an indicator of the circulation intensity and direction in each layer.

To identify the major forcings of circulation, the layer-integrated vorticity equation in each layer is expressed as,

$$\overbrace{\int_A \left(\nabla \times \int_{\boldsymbol{Lb}}^{\boldsymbol{Lu}} \frac{\partial \vec{\boldsymbol{V}}}{\partial t} \mathbf{dz}\right) \mathbf{dA}}^{\xi_{accel}} = \overbrace{\int_A \left(\nabla \times \int_{\boldsymbol{Lb}}^{\boldsymbol{Lu}} -\vec{\boldsymbol{V}} \cdot \nabla \vec{\boldsymbol{V}} \mathbf{dz}\right) \mathbf{dA}}^{\xi_{adv}} + \overbrace{\int_A \left(\nabla \times \int_{\boldsymbol{Lb}}^{\boldsymbol{Lu}} \vec{f} \times \vec{\boldsymbol{V}} \mathbf{dz}\right) \mathbf{dA}}^{\xi_{cor}} + \overbrace{\int_A \left(\nabla \times \int_{\boldsymbol{Lb}}^{\boldsymbol{Lu}} -\frac{1}{\rho_0} \nabla P \mathbf{dz}\right) \mathbf{dA}}^{\xi_{pgf}} + \overbrace{\underbrace{\int_A \nabla \times \frac{\tau_s}{\rho_0} \mathbf{dA}}_{\xi_{sstr}} - \underbrace{\int_A \nabla \times \frac{\tau_b}{\rho_0} \mathbf{dA}}_{\xi_{sstr}}}^{\xi_{visc}} \tag{2}$$

where f is the Coriolis parameter, ρ_0 is the density, and P is the pressure. ξ_{accel} is layer-integrated changing rate of vorticity and ξ_{adv} is the combination of horizontal relative vorticity advection and tilting. According to the divergence theorem, ξ_{cor} denotes the net lateral planetary vorticity flux through the straits. ξ_{pgf} is the bottom pressure torque induced by the interaction of flow and topography. The vertical viscosity ξ_{visc} could be divided into the surface ξ_{sstr} and bottom stress curl ξ_{bstr} in each specific layer. It represents wind stress (τ_s) and bottom frictional stress (τ_b) curls in the upper and deep layers, respectively.

3. Results and discussion

3.1. Regime transition of the layered circulation

The domain-averaged vorticity in the upper ($\mathbf{\Gamma}^{\boldsymbol{U}} > 0$), middle ($\mathbf{\Gamma}^{\boldsymbol{M}} < 0$), and deep ($\mathbf{\Gamma}^{\boldsymbol{D}} > 0$) layers provides quantitative insights into the evolution of the layered circulation in the SCS. In this context, an increasing (decreasing) vorticity trend in the upper and deep layers corresponds to a strengthening (weakening) of cyclonic circulation, while in the middle layer, an increasing (decreasing) vorticity trend reflects the weakening (strengthening) of the anticyclonic circulation. These variations exhibit contrasting temporal variations and changing regimes across two periods: pre-2009 (1993–2008) and post-2009 (2009–2018) (Fig. 2). Specifically, the regime transition between pre-2009 and post-2009 is characterized by strengthening and weakening trends of upper-layer circulation, and by weakening and strengthening trend of middle-layer circulation, respectively. It is also shown by a pronounced intensification of deep-layer circulation during post-2009.

This regime transition is strongly associated with the external climatic oscillation from the Pacific Decadal Oscillation (PDO) and internal dynamics arising from flow-topography interactions. During the negative phase of PDO, the easterly wind anomaly develops over the tropical WPO, strengthening the North Equatorial Current and KC [2,40,41], which in turn reduces the intrusion through the Luzon Strait. Over the SCS basin, the wind forcing shows a cyclonic anomaly [25,42]. Thus, during the negative phase of PDO, the wind stress curl (WSC) and the planetary vorticity flux through the Luzon Strait contribute positive and negative anomalies to cyclonic circulation in the SCS (Fig. 2a). Conversely, the opposite pattern occurs during the positive phase of the PDO.

Modulated by these changing external atmospheric forcing and the lateral planetary vorticity fluxes, the upper-layer circulation undergoes a significant transition, corresponding closely to the phase shift of PDO (Fig. 2a). During the pre-2009 period, when PDO index shifts from positive to negative phase, the upper-layer circulation exhibits a clear strengthening trend, with an intensification rate of approximately 6% per decade. This trend also shows strong negative correlation between the PDO index and $\mathbf{\Gamma}^{\boldsymbol{U}}$, with a coefficient ($\boldsymbol{r}$) of –0.91. Over the central SCS basin, a rising trend in sea surface height was also observed prior to 2009, which reflects an anticyclonic trend in surface geostrophic circulation [24,43]. Since the present analysis focuses on the basin-integrated circulation in the entire upper layer and includes the effects of ageostrophic processes such as wind forcing, the strengthening trend identified here may differ from the localized anticyclonic tendencies in earlier studies. Conversely, during the post-2009 period when the PDO index shifts from a negative to positive phase, the trend of upper-layer circulation reverses, weakening at a slower rate of approximately –2% per decade. Concurrently, the correlation between $\mathbf{\Gamma}^{\boldsymbol{U}}$ and PDO index gradually becomes positive, particularly after 2010 when $\boldsymbol{r}$ reaches 0.72.

In the middle layer, the changing trend broadly mirrors that of the upper layer (Fig. 2b). During pre-2009 period, negative $\mathbf{\Gamma}^{\boldsymbol{M}}$ exhibits a positive trend that the vorticity increases by approximately 3% per decade. Given that the middle-layer circulation flows in an anticyclonic direction with negative vorticity, this positive trend suggests a weakening of the circulation. However, in the post-2009 period, the trend reverses with anticyclonic circulation strengthening at a much higher rate of approximately 13% per decade. Additionally, on the sub-decadal scale, a robust negative correlation is noted between the upper- and middle-layer circulations. The detrended $\mathbf{\Gamma}^{\boldsymbol{M}}$ and $\mathbf{\Gamma}^{\boldsymbol{U}}$ in pre-2009 and post-2009 yield correlation coefficients of –0.72 and –0.60, respectively (Fig. S4 online). This suggests that, on the sub-decadal scale, a stronger upper-layer circulation is typically accompanied by a stronger middle-layer anticyclonic circulation. This indicates a possible vertical coupling for transmitting climatic variability from upper-layer circulation [18,44–46].

In the deep layer (Fig. 2c), the circulation does not exhibit a significantly changing trend during the pre-2009 period. However, it strengthened substantially during the post-2009 period, with an increase rate of approximately 15% per decade. As shown in previous studies, the density difference across the Luzon Strait induces a westward pressure gradient, driving the deep intrusion from the WPO into the SCS and maintaining the deep-layer cyclonic circulation [14,17,44]. The observed data on crossing Luzon Strait density

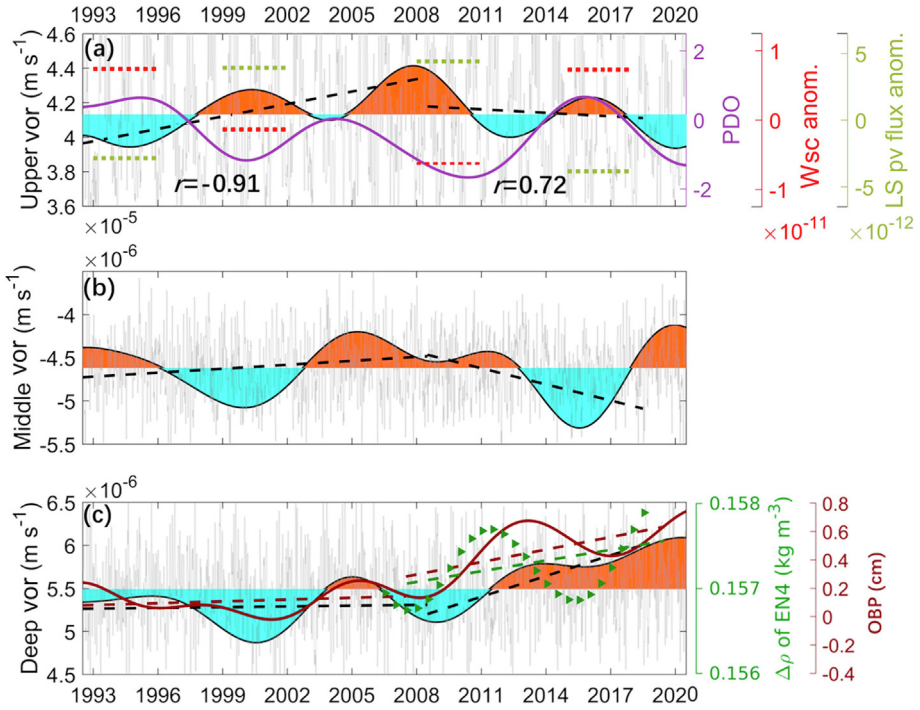

Fig. 2. Transition in changing regime of the layered circulation in SCS. (a) Smoothed (7-year) upper layer domain-averaged vorticity (color, positive Γ^U) and PDO index (purple line) during two regimes pre-2009 (1993–2008, R1) and post-2009 (2009–2018, R2). The black dashed lines show the linear trend of Γ^U during pre-2009 and post-2009, and the gray line represents the unsmoothed upper layer vorticity. The red and green horizontal lines represent the wind stress curl (WSC) and horizontal planetary vorticity flux through the Luzon Strait (LS pv flux) anomalies during the positive phase (solid) and negative phase (dashed) of PDO. (b) Smoothed (7-year) middle layer domain-averaged vorticity (color, negative Γ^M). The black dashed lines show the linear trend of Γ^M during pre-2009 and post-2009, and the gray line represents the unsmoothed middle layer vorticity. (c) Smoothed (7-year) deep layer domain-averaged vorticity (color, positive Γ^D), the density difference across the Luzon Strait in EN4 data (green triangles) and OBP across the LS (red line). The dashed lines show their linear trends during pre-2009 and post-2009, and the gray line represents the unsmoothed deep layer vorticity.

difference, bottom pressure difference (OBP) (Fig. 2c) and the deep overflow from WPO through the Luzon Strait [3], primarily available in post-2009 period, consistently indicate a significant enhancement. This is consistent with the strengthening of the deep-layer circulation. It is worth noting that some previous studies have reported opposite decadal trends in the deep overflow through Luzon Strait during this period [3,47,48]. Such inconsistencies highlight the complexity of the SCS deep-layer circulation system and the limitations imposed by sparse long-term observations. The coarse resolution and depth mismatches in the data may obscure signals in narrow straits or regions with steep topography, thus complicating interpretation. The results presented here should therefore be viewed in this context, emphasizing the need for sustained, basin-scale monitoring.

3.2. External and internal drivers of circulation regime transition

To better understand the decadal regime transition in SCS, the underlying physical drivers are quantitatively examined using the layered-integrated vorticity budget [7,9,34]. For the mean layered CAC circulation, the system is primarily governed by the interplay between the external planetary vorticity flux across the basin's lateral boundary (ξ_{cor}), and the internal bottom pressure torque induced by the flow-topography interaction [49] (ξ_{pgf}). In addition, the upper-layer circulation is further maintained by the vorticity input from surface WSC (ξ_{sstr}) (Fig. 3a).

In the upper layer, two major drivers of the basin circulation and its decadal variability are surface WSC and lateral planetary vorticity flux, both of which exhibit a regime transition across two periods (Fig. 3b). During pre-2009 period when the PDO transitions from a positive to a negative phase, the WSC over the SCS shifts from an anticyclonic to a cyclonic anomaly (Fig. 2a), producing a positive trend of 6.3×10^{-12} m s^{-2} decadal^{-1}. Concurrently, the transition of wind forcing over the WPO results in a decreasing trend in planetary vorticity input to the SCS of -3.7×10^{-12} m s^{-2} decadal^{-1} [50]. These trends reverse during the post-2009 period that WSC weakens substantially to -2.1×10^{-11} m s^{-2} decadal^{-1}, whereas the lateral planetary vorticity flux strengthens to 1.6×10^{-11} m s^{-2} decadal^{-1}. Although the Luzon Strait remains the dominant source of lateral planetary vorticity flux, PDO-related signals transmitted through the Mindoro Strait strongly influence the regime shifts in SCS sea level [24], which may in turn modulate upper-layer circulation. This suggests that the Mindoro Strait serves as a complementary pathway that warrants further investigation.

Across two regimes, the decadal changing trend of upper-layer circulation is mainly controlled by WSC. Beyond the linear trends within each period, it is also noted that Γ^U is positively correlated with WSC in pre-2009 period with r = 0.85. However, in the post-2009 period, as upper intrusion through the Luzon Strait intensifies and surface WSC weakens, lateral planetary vorticity flux begins to play a more significant role in modulating the sub-decadal variability of upper-layer circulation, with r =0.46. This shift also explains why the correlation between Γ^U and the PDO index transits from negative to positive across the two periods (Fig. 2a).

In the middle layer (Fig. 3c), the weakening trend of circulation during pre-2009 is primarily controlled by the bottom pressure torque, as indicated by the strong positive correlation between ξ^M_{pgf} and Γ^M (r = 0.92). The bottom pressure torque arises from the interaction between the bottom pressure gradient and sloping topography, constraining geostrophic flow along isobaths. Although bottom pressure torque does not alter the potential vor-

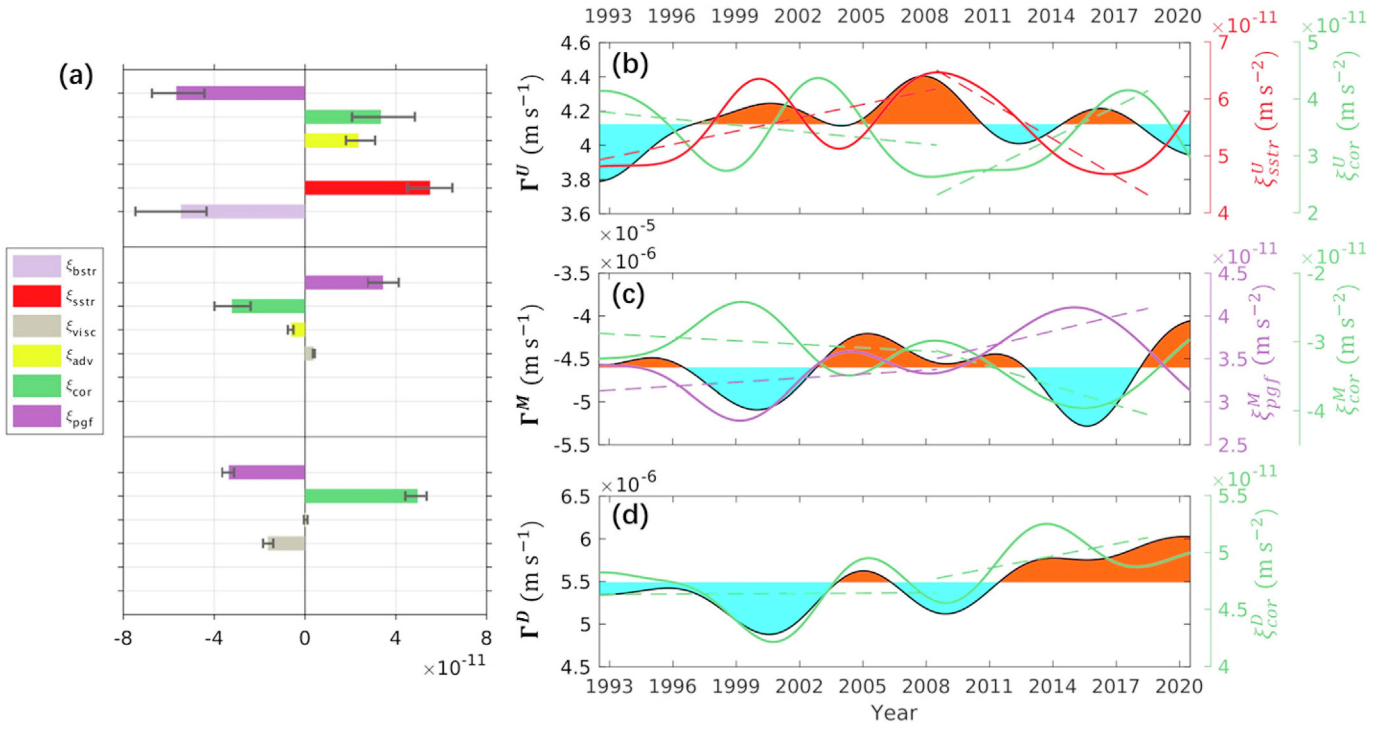

Fig. 3. Vorticity budget during the circulation regime transition. (a) The mean terms in layered-integrated vorticity equation in the upper, middle and deep layers. ξ_{cor} indicates vortex stretching/squeezing, which is the equivalent to planetary vorticity flux across the open boundary [7], ξ_{adv} is horizontal advection and titling, ξ_{pgf} is the bottom pressure torque, ξ_{visc} is the turbulent viscosity; ξ_{sstr} and ξ_{bstr} are the surface and bottom stress curl for each layer. For upper layer, the ξ_{sstr} is the surface wind stress curl. (b) Smoothed (7-year) domain-averaged vorticity (color, $\mathbf{\Gamma^U}$), $\xi^{\mathbf{U}}_{sstr}$ (red line) and $\xi^{\mathbf{U}}_{cor}$ (blue line) in upper layer. The dashed lines show the linear trend during pre-2009 and post-2009, respectively. (c) Smoothed (7-year) domain-averaged vorticity (color, $\mathbf{\Gamma^M}$), $\xi^{\mathbf{M}}_{pgf}$ (purple line) and $\xi^{\mathbf{M}}_{cor}$ (green line) in middle layer. The dashed lines show the linear trend of $\xi^{\mathbf{M}}_{pgf}$ and $\xi^{\mathbf{M}}_{cor}$ during pre-2009 and post-2009, respectively. (d) Smoothed (7-year) domain-averaged vorticity (color, $\mathbf{\Gamma^D}$) and $\xi^{\mathbf{D}}_{cor}$(green line) in deep layer. The dashed lines show the linear trend $\xi^{\mathbf{D}}_{cor}$ during pre-2009 and post-2009, respectively.

ticity of individual water parcels, it reflects vertical motion induced by bottom geostrophic cross-isobath transport, which can impose a squeezing effect on the overlying flow. The variations in bottom pressure torque are closely tied to the bottom pressure distribution, which in turn is shaped by motions throughout the entire water column. During this period, the intensification of bottom pressure torque is associated with the strengthening of the upper-layer circulation. It suggests that the upper layer can exert a significant influence on the decadal variation and trend of the middle-layer circulation by modulating the bottom pressure pattern [46]. In the post-2009 period, however, the strengthening trend of the middle-layer circulation becomes controlled by the negative trend of lateral planetary vorticity flux, as reflected in a positive correlation between $\xi^{\mathbf{M}}_{cor}$ and $\mathbf{\Gamma^M}$ ($\boldsymbol{r}$ = 0.91). In the semi-enclosed basin, the lateral transport of vorticity corresponds to internal vortex stretching in the water column. It is also noteworthy that the horizontal pattern of decadal changing trend in ξ^{D}_{cor} closely resembles that of $\xi^{\mathbf{M}}_{cor}$ (Fig. S5g and k online). Thus, the changes in $\xi^{\mathbf{M}}_{cor}$ in the middle layer are supported by the concurrent increasing trend of ξ^{D}_{cor} in the semi-enclosed deep layers. This alignment highlights the vertically coupled nature of the circulation system, which modulates the middle layer's response to changes in entire layered circulation. During the transition between dominant mechanisms, the correlation between the upper- and middle-layer vorticities weakens, as seen during the 2005–2010 period (Fig. 2 and Fig. S4 online).

For the deep-layer circulation, both the decadal changing trend and the sub-decadal variability are controlled by planetary vorticity input by the deep intrusion through the Luzon Strait. Notably, in the post-2009 period, the intensification of planetary vorticity input (as shown in Figs. 2c and 3d) imposes stronger vortex squeezing on the middle layer. This interaction supports the strengthening trend of middle-layer anticyclonic circulation during this period.

4. Conclusion

Using a combination of high-resolution numerical simulations and observational data, this study explores the decadal regime transition of unique rotating layered circulation in the largest marginal sea of the Pacific Ocean (Fig. 4). The result identifies two distinct circulation regimes in the SCS, each closely linked to phase shifts in the PDO and characterizes by contrasting forcing conditions.

During pre-2009 period, the upper-layer cyclonic circulation strengthened, while the middle-layer anticyclonic circulation weakened. In contrast, during the post-2009 period, these trends reverse and are accompanied by a pronounced intensification of deep-layer cyclonic circulation. These transitions reflect a structural reorganization of the SCS interior circulation, driven by evolving external forcings and internal response dynamics.

The analysis highlights the interplay of surface wind forcing, external exchanging current with the Pacific, and topographically modulated internal vertical coupling in shaping the long-term evolution and decadal variability of basin circulation (Fig. 4). Across the two regimes, the decadal trend of the upper-layer circulation is primarily controlled by wind forcing. While in the middle layer, the weakening of circulation during pre-2009 is mainly governed by the bottom pressure torque, which is influenced by the strengthening of the upper-layer circulation. In contrast, during the post-2009 period, the strengthening trend in the middle layer is largely driven by the vortex stretching, which is supported by

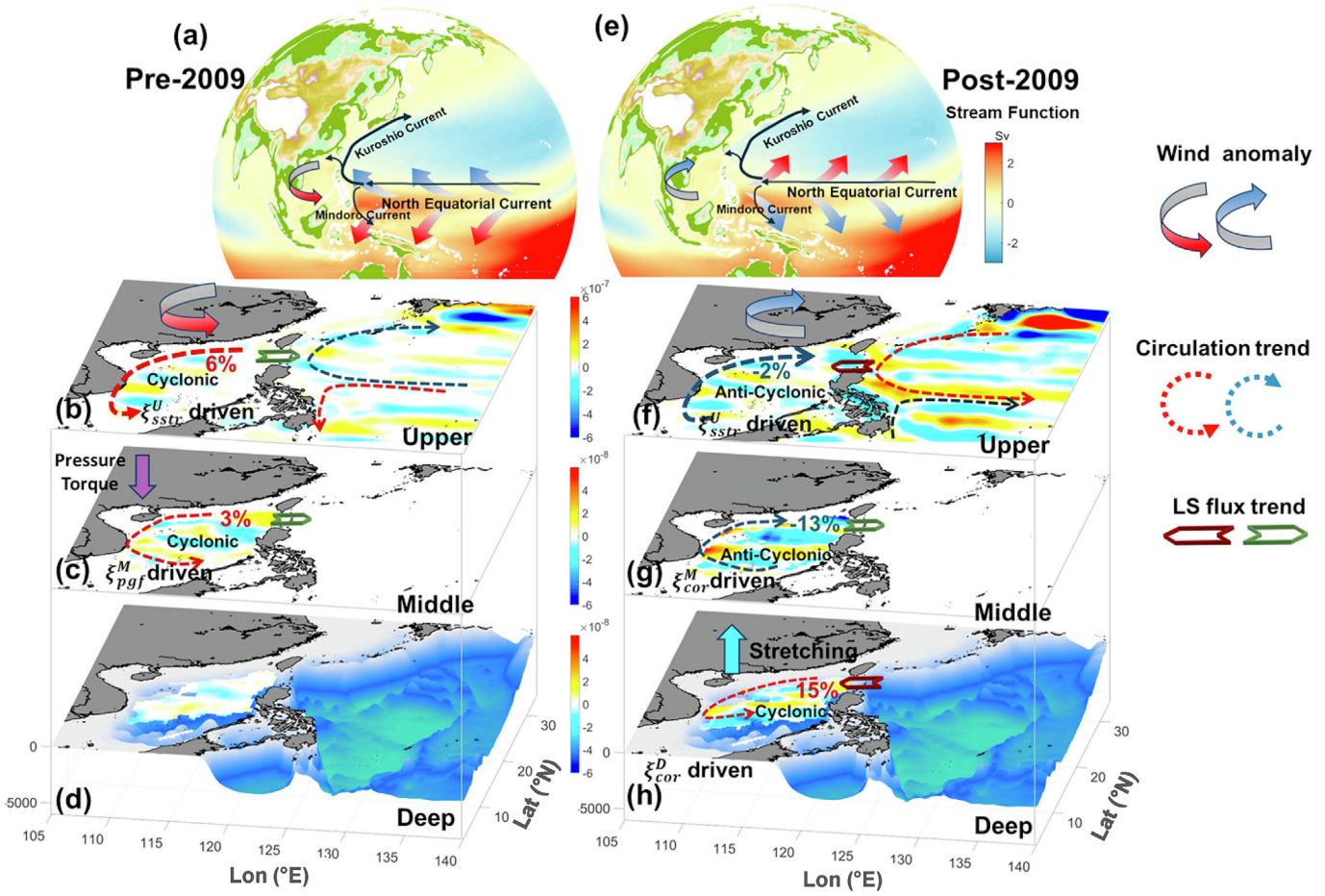

Fig. 4. Schematic representation of the regime transition of the South China Sea-Western Pacific circulation. (a) Surface streamfunction derived from CMEMS data during pre-2009 period and the changing trend of wind forcing. (b–d) The linear trend of layered circulation (dashed arrows) and the Luzon Strait flux (red and green hollow arrows) during pre-2009 period in each layer. The changing trend in upper-layer cyclonic circulation and middle-layer anticyclonic circulation is controlled by the ξ^{U}_{sstr} and ξ^{M}_{pgf}, respectively. The purple downward arrow represents the effect of bottom pressure torque imposed on the middle layer. (e–h) are the same as (a–d) but for the post-2009 period. During the post-2009 period, the changing trend in upper-layer cyclonic circulation, middle-layer anticyclonic circulation, and deep-layer cyclonic circulation is controlled by the ξ^{U}_{sstr}, ξ^{M}_{cor}, and ξ^{D}_{cor}, respectively. The light blue arrow represents the impact of vertical stretching imposed on the middle layer

the increased stretching in the semi-enclosed deep layer. This highlights the vertically coupled nature of the layered circulation system in SCS, which governs the middle layer's response to changes in the entire layered circulation. For the deep layer, the changes in circulation are predominantly controlled by deep-water intrusion through the Luzon Strait. The findings advance understanding of how SCS circulation adjusts to climate variability and modulates regional heat and salt transport, nutrient cycling, and ocean–atmosphere interactions.

Although this study primarily adopts a geopotential level based vorticity analysis, future investigations incorporating isopycnal dynamics and related potential vorticity could yield insight into regime transitions in the layered circulation [16,51,52]. Potential vorticity based analysis offers a powerful framework that unifies the effects of rotation, stratification, and column stretching. Stratification may further influence the structure and intensity of circulation, as suggested by recent studies [53,54]. Investigating these processes within an isopycnal framework represents a valuable direction for future research.

Conflict of interest

The authors declare that they have no conflict of interest.

Acknowledgments

This work was supported by the National Natural Science Foundation of China (42376024 and 42450181) and the Science and Technology Development Fund, Macau SAR (File/Project no. 001/2024/SKL). This work was also supported by the Centre for Regional Oceans in the University of Macau (SP2025-00005-CRO), and CORE, which is a joint research center for ocean research between Laoshan Laboratory and HKUST, and substantially supported by a grant from the Research Grants Council of the Hong Kong Special Administrative Region, China (AoE/P-601/23-N and GRF 16310724). We are also grateful for the support of the National Supercomputing Centers of Guangzhou and Tianjin. This work was performed in part at the SICC, which is supported by the SKL-IOTSC, University of Macau

Author contributions

Lixia Zheng conducted the data analysis and drafted the figures and manuscript. Zhongya Cai and Jianping Gan revised and supervised the manuscript. Chiwing Hui, Linlin Liang, Hiusuet Kung, and Zhiqiang Liu performed the numerical simulations and interpreted the results.

Data availability

The CMOMS data are available at https://odmp.ust.hk/cmoms/. The data from NOAA are available at https://www.ncdc.noaa.gov/oa/rsad/air-sea/seawinds.html. The data from OFES are available at http://apdrc.soest.hawaii.edu/ESC/escdata_main.php. The data from CMEMS are available at https://data.marine.copernicus.eu/product/SEALEVEL_GLO_PHY_L4_MY_008_047/description. The data from EN4 are available at https://climatedataguide.ucar.edu/climate-data/en4-subsurface-temperature-and-salinity-global-oceans.

Appendix A. Supplementary material

Supplementary data to this article can be found online at https://doi.org/10.1016/j.scib.2025.12.033.

References

[1] Gan J, Li H, Curchitser E, et al. Modeling South China Sea circulation: response to seasonal forcing regimes. J Geophys Res 2006;111:1–20.
[2] Hu D, Wu L, Cai W, et al. Pacific western boundary currents and their roles in climate. Nature 2015;522:299–308.
[3] Zhou C, Xiao X, Zhao W, et al. Increasing deep-water overflow from the Pacific into the South China Sea revealed by mooring observations. Nat Commun 2023;14:2013.
[4] Tozuka T, Qu T, Yamagata T. Dramatic impact of the South China Sea on the Indonesian throughflow. Geophys Res Lett 2007;34:L12612.
[5] Qu T, Song YT, Yamagata T. An introduction to the South China Sea throughflow: its dynamics, variability, and application for climate. Dynam Atmos Oceans 2009;47:3–14.
[6] Gordon AL, Huber BA, Metzger EJ, et al. South China Sea throughflow impact on the Indonesian throughflow. Geophys Res Lett 2012;39:L11602.
[7] Gan J, Kung H, Cai Z, et al. Hotspots of the stokes rotating circulation in a large marginal sea. Nat Commun 2022;13:2223.
[8] Gan J, Liu Z, Liang L. Numerical modeling of intrinsically and extrinsically forced seasonal circulation in the China Seas: a kinematic study. J Geophys Res Oceans 2016;121:4697–715.
[9] Gan J, Liu Z, Hui CR. A three-layer alternating spinning circulation in the South China Sea. J Phys Oceanogr 2016;46:2309–15.
[10] Zhu Y, Sun J, Wang Y, et al. Overview of the multi-layer circulation in the South China Sea. Prog Oceanogr 2019;175:171–82.
[11] Cai Z, Gan J, Liu Z, et al. Progress on the formation dynamics of the layered circulation in the South China Sea. Prog Oceanogr 2020;181:102246.
[12] Lan J, Zhang N, Wang Y. On the dynamics of the South China Sea deep circulation. J Geophys Res 2013;118:1206–10.
[13] Xu F-H, Oey L-Y. State analysis using the Local Ensemble Transform Kalman Filter (LETKF) and the three-layer circulation structure of the Luzon Strait and the South China Sea. Ocean Dyn 2014;64:905–23.
[14] Wang G, Xie SP, Qu T, et al. Deep South China Sea circulation. Geophys Res Lett 2011;38:1–6.
[15] Yuan D. A numerical study of the South China Sea deep circulation and its relation to the Luzon Strait transport. Acta Oceanol Sin 2002;21:187–202.
[16] Zhu Y, Sun J, Wang Y, et al. Effect of potential vorticity flux on the circulation in the South China Sea. J Geophys Res Oceans 2017;122:6454–69.
[17] Tian J, Yang Q, Liang X, et al. Observation of Luzon Strait transport. Geophys Res Lett 2006;33:1–6.
[18] Quan Q, Xue H. Layered model and insights into the vertical coupling of the South China Sea circulation in the upper and middle layers. Ocean Model 2018;129:75–92.
[19] Liu Q, Feng M, Wang D. ENSO-induced interannual variability in the southeastern South China Sea. J Oceanogr 2011;67:127–33.
[20] Jing Z, Qi Y, Du Y. Upwelling in the continental shelf of northern South China Sea associated with 1997–1998 El Niño. J Geophys Res Oceans 2011;116.
[21] Xie S-P, Hu K, Hafner J, et al. Indian ocean capacitor effect on Indo–Western Pacific climate during the summer following El Niño. J Clim 2009;22:730–47.
[22] Chen CTA, Guo X. Changing Asia-Pacific Marginal Seas. Springer Singapore; 2020.
[23] Yu K, Qu T. Imprint of the Pacific decadal oscillation on the South China Sea throughflow variability. J Clim 2013;26:9797–805.
[24] Cheng X, Zhao M, Duan W, et al. Regime shift of the sea level trend in the South China Sea modulated by the tropical Pacific decadal variability. Geophys Res Lett 2023;50:e2022GL102708.
[25] Cheng X, Xie S-P, Du Y, et al. Interannual-to-decadal variability and trends of sea level in the South China Sea. Clim Dyn 2016;46:3113–26.
[26] Chen Y, Zhai F, Li P. Decadal variation of the Kuroshio intrusion into the South China Sea during 1992–2016. J Geophys Res Oceans 2020;125:e2019JC015699.
[27] Team BA. Assessment of climate change for the Baltic Sea basin. Springer Science & Business Media; 2008.
[28] Millot C, Taupier-Letage I. Circulation in the Mediterranean Sea. In: Saliot A, editor. The Mediterranean Sea. Handbook of Environmental Chemistry, vol 5K. Berlin: Springer; 2005, p. 29–66.
[29] Furey H, Bower A, Perez-Brunius P, et al. Deep eddies in the Gulf of Mexico observed with floats. J Phys Oceanogr 2018;48:2703–19.
[30] Hu S, Sprintall J, Guan C, et al. Deep-reaching acceleration of global mean ocean circulation over the past two decades. Sci Adv 2020;6:eaax7727.
[31] Forget G, Ferreira D. Global ocean heat transport dominated by heat export from the tropical Pacific. Nat Geosci 2019;12:351–4.
[32] Desbruyères D, Chafik L, Maze G. A shift in the ocean circulation has warmed the subpolar North Atlantic ocean since 2016. Commun Earth Environ 2021;2:48.
[33] Sumata H, de Steur L, Divine DV, et al. Regime shift in Arctic ocean sea ice thickness. Nature 2023;615:443–9.
[34] Wang Q, Zeng L, Chen J, et al. Phase shift of the winter South China Sea Western boundary current over the past two decades and its drivers. Geophys Res Lett 2023;50:e2023GL103145.
[35] del Monte-Luna P, Villalobos H, Arreguín-Sánchez F. Variability of sea surface temperature in the southwestern Gulf of Mexico. Cont Shelf Res 2015;102:73–9.
[36] Civitarese G, Gačić M, Lipizer M, et al. On the impact of the Bimodal Oscillating System (BiOS) on the biogeochemistry and biology of the Adriatic and Ionian Seas (Eastern Mediterranean). Biogeosciences 2010;7:3987–97.
[37] Lavigne H, Civitarese G, Gačić M, et al. Impact of decadal reversals of the north Ionian circulation on phytoplankton phenology. Biogeosciences 2018;15:4431–45.
[38] Shchepetkin AF, McWilliams JC. The regional oceanic modeling system (ROMS): a split-explicit, free-surface, topography-following-coordinate oceanic model. Ocean Model 2005;9:347–404.
[39] Cai Z, Gan J. Dynamics of the layered circulation inferred from kinetic energy pathway in the South China Sea. J Phys Oceanogr 2021;51:1671–85.
[40] Wu C-R. Interannual modulation of the Pacific Decadal Oscillation (PDO) on the low-latitude western North Pacific. Prog Oceanogr 2013;110:49–58.
[41] Qiu B, Chen S. Interannual-to-decadal variability in the bifurcation of the north equatorial current off the Philippines. J Phys Oceanogr 2010;40:2525–38.
[42] Merrifield MA, Thompson PR, Lander M. Multidecadal sea level anomalies and trends in the western tropical Pacific. Geophys Res Lett 2012;39.
[43] Fang W, Qiu F, Guo P. Summer circulation variability in the South China Sea during 2006–2010. J Mar Syst 2014;137:47–54.
[44] Cai Z, Chen D, Gan J. Formation of the layered circulation in South China Sea with the mixing stimulated exchanging current through Luzon Strait. J Geophys Res Oceans 2023;126:e2023JC019730.
[45] Cai Z, Gan J. Dynamics of the cross-layer exchange for the layered circulation in the South China Sea. J Geophys Res Oceans 2020;125:e2020JC016131.
[46] Tang Q, Cai Z, Liu Z. Topographic modulation on the layered circulation in South China Sea. Ocean Sci 2025;21:1291–301.
[47] Zhu Y, Yao J, Xu T, et al. Weakening trend of luzon strait overflow transport in the past two decades. Geophys Res Lett 2022;49:e2021GL097395.
[48] Zhu Y, Yao J, Li S, et al. Decadal weakening of abyssal South China Sea circulation. Geophys Res Lett 2022;49:e2022GL100582.
[49] Mertz G, Wright DG. Interpretations of the JEBAR term. J Phys Oceanogr 1992;22:301–5.
[50] Nan F, Xue H, Yu F. Kuroshio intrusion into the South China Sea: a review. Prog Oceanogr 2015;137:314–33.
[51] Yang J, Price JF. Water-mass formation and potential vorticity balance in an abyssal ocean circulation. J Mar Res 2000;58:789–808.
[52] Yang J. The Arctic and Subarctic ocean flux of potential vorticity and the Arctic ocean circulation. J Phys Oceanogr 2005;35:2387–407.
[53] Peng Q, Xie SP, Wang D, et al. Surface warming-induced global acceleration of upper ocean currents. Sci Adv 2022;8:eabj8394.
[54] Rahmstorf S, Box JE, Feulner G, et al. Exceptional twentieth-century slowdown in Atlantic ocean overturning circulation. Nat Clim Change 2015;5:475–80.